Technical Note on CERES EBAF Ed2.7

TOA Outgoing Longwave Radiation (rlut)
TOA Outgoing Clear-Sky Longwave Radiation (rlutcs)
TOA Outgoing Shortwave Radiation (rsut)
TOA Outgoing Clear-Sky Shortwave Radiation (rsutcs)

1. Intent of This Document and POC

1a) This document is intended for users who wish to compare CMIP5/IPCC historical climate model output with satellite-derived observations. Users are not expected to be experts in satellite-derived Earth system observational data. This document summarizes essential information needed for comparing this dataset to climate model output. References are provided at the end of this document to additional information.

This NASA dataset is provided as part of an experimental activity to increase the usability of NASA satellite observational data for the modeling and model analysis communities. This is not a standard NASA satellite instrument product, but does represent an effort on behalf of data experts to identify a product that is appropriate for routine model evaluation. The data may have been reprocessed, reformatted, or created solely for comparisons with climate model output. Community feedback to improve and validate the dataset for modeling usage is appreciated. Email comments to HQ-CLIMATE-OBS@mail.nasa.gov.

Dataset File Name (as it appears on the ESGF):

rlut_CERES-EBAF_L3B_Ed2-7_200003-201304.nc
rlutcs_CERES-EBAF_L3B_Ed2-7_200003-201304.nc
rsut_CERES-EBAF_L3B_Ed2-7_200003-201304.nc
rsutcs_CERES-EBAF_L3B_Ed2-7_200003-201304.nc

1b) Technical point of contact for this dataset:

Norman Loeb email: Norman.G.Loeb@nasa.gov

2. Data Field Description

CF variable name, units:	TOA Outgoing Longwave Radiation (rlut), W m^{-2} TOA Outgoing Clear-Sky Longwave Radiation (rlutcs), W m^{-2} TOA Outgoing Shortwave Radiation (rsut), W m^{-2} TOA Outgoing Clear-Sky Shortwave Radiation (rsutcs), W m^{-2}
Spatial resolution:	1°x1° latitude by longitude
Temporal resolution and extent:	Monthly averaged from 03/2000 to 04/2013
Coverage:	Global

3. Data Origin

CERES instruments fly on the Terra (descending sun-synchronous orbit with an equator crossing time of 10:30 A.M. local time) and Aqua (ascending sun-synchronous orbit with an equator crossing time of 1:30 P.M. local time) satellites. Each CERES instrument measures filtered

radiances in the shortwave (SW; wavelengths between 0.3 and 5 μm), total (TOT; wavelengths between 0.3 and 200 μm), and window (WN; wavelengths between 8 and 12 μm) regions. To correct for the imperfect spectral response of the instrument, the filtered radiances are converted to unfiltered reflected solar, unfiltered emitted terrestrial longwave (LW) and window (WN) radiances (Loeb et al. 2001). Since there is no LW channel on CERES, LW daytime radiances are determined from the difference between the TOT and SW channel radiances. Instantaneous top-of-atmosphere (TOA) radiative fluxes are estimated from unfiltered radiances using empirical angular distribution models (ADMs; Loeb et al. 2003, 2005) for different scene types identified using retrievals from Moderate Resolution Imaging Spectrometer (MODIS) measurements (Minnis et al. 2011). Monthly mean fluxes are determined by spatially averaging the instantaneous values on a 1°×1° grid, temporally interpolating between observed values at 1-h increments for each hour of every month, and then averaging all hour boxes in a month. Level-3 processing is performed on a nested grid, which uses 1° equal-angle regions between 45°N and 45°S, maintaining area consistency at higher latitudes. The fluxes from the nested grid are then output to a complete 360x180 1°×1° grid created by replication.

Monthly regional CERES LW and SW TOA fluxes in the CMIP5 archive are from the CERES Energy Balanced and Filled (EBAF) Ed2.7 data product. This version differs from EBAF Ed1.0 (Loeb et al. 2009) in many respects. The LW and SW TOA fluxes in EBAF Ed2.7 are derived from two standard gridded daily CERES products that utilize complementary time interpolation methods:

(i) SSF1deg_Ed2.7: The LW fluxes in each hour box between CERES observations are determined by linear interpolation of LW fluxes over ocean, while daytime and nighttime observations over land and desert are interpolated by fitting a half-sine curve to the observations to account for the much stronger diurnal cycle over land and desert (Young et al. 1998). The SW radiative fluxes between CERES observation times are determined from the observed fluxes by using scene-dependent diurnal albedo models to estimate how TOA albedo (and therefore flux) changes with solar zenith angle for each local time, assuming the scene properties remain invariant throughout the day. The sun angle–dependent diurnal albedo models are based upon the CERES ADMs developed for the Tropical Rainfall Measuring Mission (TRMM) satellite (Loeb et al. 2003).

(ii) SYN1deg_Ed2.7: SW and LW radiative fluxes between CERES observation times are determined by supplementing the CERES observations with 3-hourly TOA fluxes derived from 5 geostationary satellites. Doelling et al. (2013) provides a detailed description of how broadband TOA fluxes are derived from geostationary data.

SSF1deg provides global coverage daily with excellent calibration stability, but samples only at specific times of the day due to the sun-synchronous orbit. While the SYN1deg approach provides improved diurnal coverage by merging CERES and 3-hourly geostationary data, artifacts in the GEO data over certain regions and time periods can introduce larger uncertainties. In order to remove most of the GEO-derived flux biases, the fluxes are normalized at Terra or Aqua observation times to remain consistent with the CERES instrument calibration (Doelling et al. 2013). Nevertheless, spurious jumps in the SW TOA flux record can still occur when GEO satellites are replaced due to changes in satellite position, calibration and/or visible sensor spectral response, and imaging schedules. Such artifacts in the GEO data can be problematic in studies of TOA radiation interannual variability and/or trends.

To maintain the excellent CERES instrument calibration stability of SSF1deg and also preserve diurnal information in SYN1deg, EBAF Ed2.7 uses a new approach involving scene dependent diurnal corrections to convert daily regional mean SSF1deg fluxes to diurnally complete values analogous to SYN1deg, but without geostationary artifacts. The diurnal corrections are ratios of SYN1deg-to-SSF1deg fluxes defined for each of the five geostationary satellite domains for each calendar month. They depend upon surface type and MODIS cloud fraction and height retrievals, and thus can vary from one day to the next along with the cloud properties (i.e., they are dynamic). For March 2000-June 2002, TOA fluxes are based upon CERES observations from the Terra spacecraft, while for July 2002 onwards, CERES SW observations from both Terra and Aqua are utilized in order to improve the accuracy of the diurnal corrections. In EBAF Ed1.0 and EBAF Ed2.5, only Terra data were used and the main input was either CERES SRBAVG GEO Edition2D or CERES SYN Ed2.5, which both explicitly rely on GEO for time interpolation. An assessment of this new approach for EBAF Ed2.7 is provided in Section 4.

The LW TOA fluxes in EBAF Ed2.7 are derived from internal versions of the CERES SYN1deg product determined for Terra only. In SYN1deg, LW radiative fluxes between CERES observation times are determined by supplementing the CERES observations with data from 5 geostationary satellites that sample every 3 hours for all longitudes between 60°S and 60°N, thus providing the most temporally and spatially complete CERES dataset for Terra or Aqua. Doelling et al. (2013) provides a detailed description of how broadband TOA fluxes are derived from geostationary data and combined with CERES observations.

The approach used to determine clear-sky TOA flux is described in detail in Loeb et al. (2009). We determine gridbox mean clear-sky fluxes using an area-weighted average of: (i) CERES/Terra broadband fluxes from completely cloud-free CERES footprints (20-km equivalent diameter at nadir), and (ii) MODIS/Terra-derived "broadband" clear-sky fluxes estimated from the cloud-free portions of partly and mostly cloudy CERES footprints. In both cases, clear regions are identified using the CERES cloud algorithm applied to MODIS 1-km pixel data (Minnis et al. 2011). Clear-sky fluxes in partly and mostly cloudy CERES footprints are derived using MODIS–CERES narrow-to-broadband regressions to convert MODIS narrowband radiances averaged over the clear portions of a footprint to broadband radiances. Separate narrow-to-broadband regressions are developed for each calendar month using all available years. The "broadband" MODIS radiances are then converted to TOA radiative fluxes using CERES clear-sky ADMs (Loeb et al. 2005). Monthly mean clear-sky TOA fluxes are determined from instantaneous values using the same approach as clear-sky fluxes in the CERES SSF1deg product described above.

As in previous versions of EBAF (Loeb et al. 2009), the CERES SW and LW fluxes in EBAF Ed2.7 are adjusted within their range of uncertainty to remove the inconsistency between average global net TOA flux and heat storage in the earth–atmosphere system, as determined primarily from ocean heat content anomaly (OHCA) data. In the current version, described in Loeb et al. (2012a), the global annual mean values are adjusted such that the July 2005–June 2010 mean net TOA flux is 0.58±0.38 W m^{-2} (uncertainties at the 90% confidence level). The uptake of heat by the Earth for this period is estimated from the sum of: (i) 0.47±0.38 W m^{-2} from the slope of weighted linear least square fit to ARGO OHCA data (Roemmich et al. 2009) to a depth of 1800 m analyzed following Lyman and Johnson (2008); (ii) 0.07±0.05 W m^{-2} from ocean heat storage at depths below 2000 m using data from 1981–2010 (Purkey and Johnson 2010), and (iii)

0.04±0.02 W m^{-2} from ice warming and melt, and atmospheric and lithospheric warming (Hansen et al. 2005; Trenberth 2009).

4. Validation and Uncertainty Estimate

Regional monthly mean CERES TOA fluxes are derived from Level-1 and -2 data. The Level-1 data correspond to calibrated radiances. Here we use the latest CERES gains and time-dependent spectral response function values (Thomas et al. 2010; Loeb et al. 2012b). The Level-2 TOA fluxes are instantaneous values at the CERES footprint scale. Their accuracy has been evaluated in several papers (Loeb et al. 2006; Loeb et al. 2007; Kato and Loeb 2005). The SSF1deg and SYN1deg products used are evaluated in Loeb et al. (2012b) and Doelling et al. (2013).

4.1 TOA Outgoing Longwave Radiation (rlut)

Figs. 1a and 1b provide regional plots of mean LW TOA flux and interannual variability for the month of March based upon all March months between 2000 and 2010. The regional standard deviation ranges from near zero at the poles to 30 W m^{-2} in the equatorial Pacific Ocean region. Considering all 1°x1° regions between 90°S×90°N, the overall regional standard deviation in LW TOA flux is 17 W m^{-2}, and the overall global mean LW TOA flux is 238 W m^{-2}.

The uncertainty in 1°x1° regional LW TOA flux is evaluated using data from 07/2002-12/2010, when CERES instruments on both Terra and Aqua were operating. We compare regional fluxes from Terra and Aqua SYN1deg directly in Fig. 2. The overall mean difference is 0.05 W m^{-2} and regional RMS difference is 2 W m^{-2}. Regional differences can reach 5 W m^{-2} in isolated regions of convection over south and central Africa and in the west Pacific Ocean region (Fig. 2b).

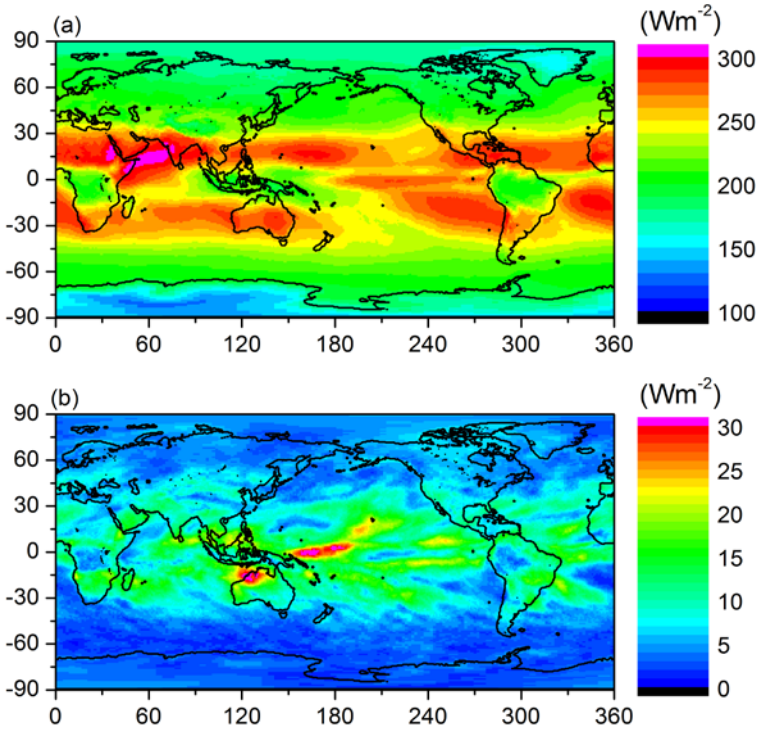

Figure 1. (a) Average and (b) standard deviation of LW TOA flux determined from all March months from 2000–2010 using the CERES EBAF Ed2.6 product.

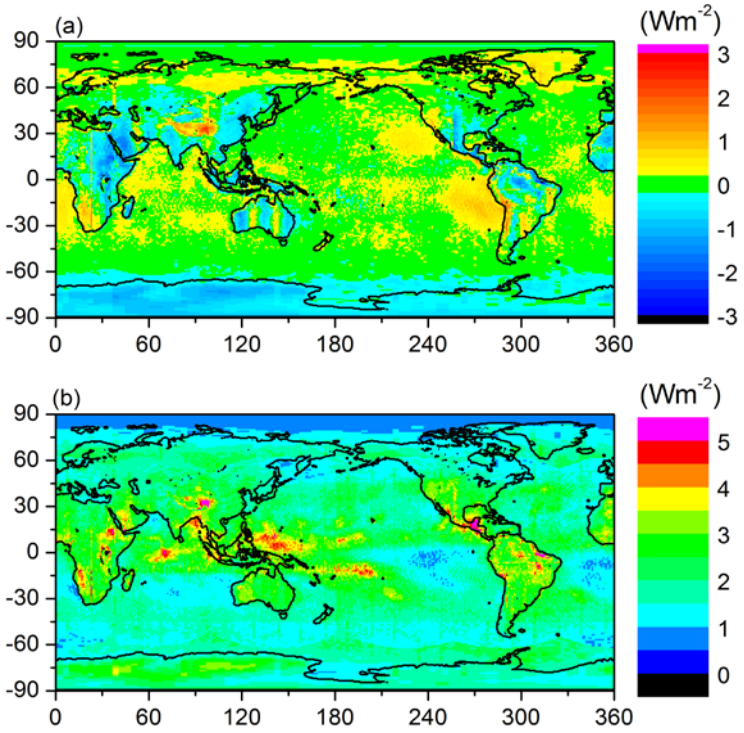

Figure 2. (a) Bias and (b) RMS difference between LW TOA fluxes from Terra and Aqua SYN1deg-lite Ed2.6 data products.

Table 1 compares global TOA averages for EBAF Ed2.7 with earlier versions of the product. All-sky LW TOA flux in Ed 2.7 and Ed2.6r is 0.1 W m^{-2} greater than Ed1.0 and Ed2.5.

Table 1. Global mean TOA fluxes (W m^{-2}) from EBAF Ed1.0, EBAF Ed2.5, EBAF Ed2.6, EBAF Ed2.6r and EBAF Ed2.7 for March 2000-February 2005 and March 2000-February 2010.

	March 2000–February 2005				
	Ed1.0	**Ed2.5**	**Ed2.6**	**Ed2.6r**	**Ed2.7**
Incoming Solar	340.0	340.2	340.5	340.0	340.0
LW (all-sky)	239.6	239.6	239.9	239.7	239.7
SW (all-sky)	99.5	99.7	100	99.8	99.8
Net (all-sky)	0.85	0.85	0.55	0.54	0.57
LW (clear-sky)	269.1	266.2	266.5	266	265.9
SW (clear-sky)	52.9	52.4	52.6	52.5	52.6
Net (clear-sky)	18.0	21.5	21.4	21.5	21.5
	March 2000–February 2010				
	Ed1.0	**Ed2.5**	**Ed2.6**	**Ed2.6r**	**Ed2.7**
Incoming Solar		340.1	340.4	339.9	339.9
LW (all-sky)		239.6	239.9	239.6	239.6
SW (all-sky)		99.5	99.9	99.7	99.7
Net (all-sky)		1.0	0.59	0.57	0.59
LW (clear-sky)		266.0	266.4	265.9	265.8
SW (clear-sky)		52.4	52.5	52.5	52.6
Net (clear-sky)		21.6	21.5	21.5	21.5

4.2 TOA Outgoing Clear-Sky Longwave Radiation (rlutcs)

Figs. 3a and 3b provide regional plots of mean clear-sky LW TOA flux and interannual variability for the month of March based upon all March months between 2000 and 2010. The 1°x1° regional standard deviation ranges from near zero at the poles to 30 W m^{-2} in mountainous regions. Considering all 1°x1° regions, the overall global regional standard deviation in clear-sky LW TOA flux is 10 W m^{-2}, and the overall global mean clear-sky LW TOA flux is 264 W m^{-2}.

The uncertainty in 1°x1° regional clear-sky LW TOA flux is determined from calibration uncertainty and errors in narrow-to-broadband conversion, radiance-to-flux conversion, time-space averaging, and scene identification. For CERES, calibration uncertainty is 0.5% (1σ), which for a typical global mean clear-sky LW flux corresponds to ≈1 W m^{-2}. Figs. 4a and 4b show the regional distribution of the correction used to offset the regional narrow-to-broadband error. This is derived by applying narrow-to-broadband regressions to MODIS infrared radiances for completely cloud-free CERES footprints and then comparing the estimated broadband flux with CERES. The overall bias is -0.5 W m^{-2}, and the regional RMS difference is 2.5 W m^{-2}. Assuming a 50% error in the correction, the narrowband-to-broadband contribution to regional uncertainty becomes 1.74 W m^{-2}. For clear-sky LW TOA flux, the radiance-to-flux conversion

error contributes 0.7 W m^{-2} to regional RMS error (Loeb et al. 2007), and time-space averaging adds 1 W m^{-2} uncertainty. The latter assumes zero error over ocean (i.e., no diurnal appreciable diurnal cycle in clear-sky LW) and a 3 W m^{-2} error in the half-sine fit over land and desert (Young et al. 1998). In EBAF, "clear-sky" is defined as cloud-free at the MODIS pixel scale (1 km). A pixel is identified as clear using spectral MODIS channel information and a cloud mask algorithm (Minnis et al. 2011). Based upon a comparison of LW TOA fluxes for CERES footprints identified as clear according to MODIS but cloudy according to CALIPSO with TOA fluxes from footprints identified as clear according to both MODIS and CALIPSO, Sun et al. (2011) found that footprints with undetected subvisible clouds emit 5.5 W m^{-2} less LW radiation compared to completely cloud-free footprints and occur in approximately 50% of footprints identified as clear by MODIS. This implies an error of 2.75 W m^{-2} due to misclassification of clear scenes. The total error in TOA outgoing clear-sky LW radiation in a region is estimated as sqrt(1^2+1.74^2+0.7^2+1^2+2.75^2) or approximately 3.6 W m^{-2}.

Table 1 compares global TOA averages for EBAF Ed2.7 with earlier versions of the product. Clear-sky LW TOA flux in Ed2.7 is 0.2—0.3 W m^{-2} smaller than Ed2.5 and 3.2 W m^{-2} smaller than Ed1.0. The main difference between EBAF Ed2.7 and Ed2.5 is that Ed2.7 applies geodetic weighting when averaging globally while geocentric weighting is assumed in EBAF Ed2.5. In EBAF Ed1.0, geocentric weighting is assumed and the methodology for time-space averaging differs from that in versions Ed2.5 and higher. Time-space averaging for the latter is now based upon the same code that is used for clear-sky LW TOA fluxes in the SSF1deg product.

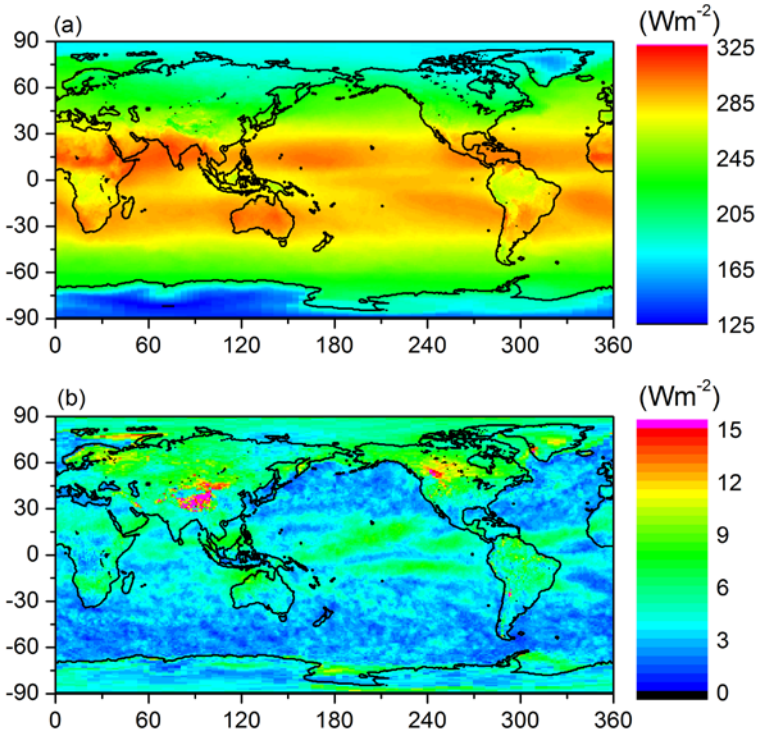

Figure 3. (a) Average and (b) standard deviation of clear-sky LW TOA flux determined from all March months from 2000–2010 using the CERES EBAF Ed2.6 product.

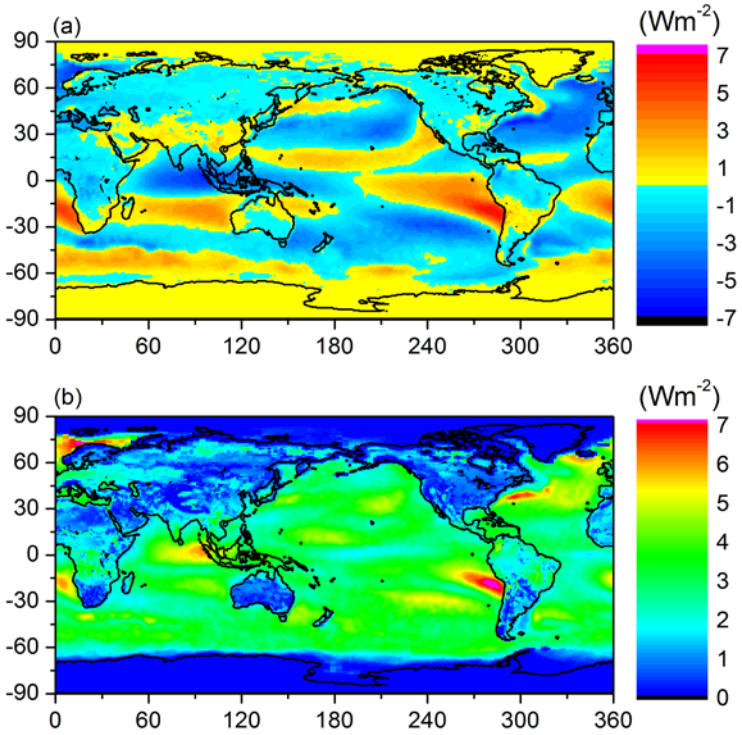

Figure 4. (a) Bias and (b) RMS difference between high-resolution clear-sky LW TOA fluxes derived with and without corrections for regional narrow-to-broadband error.

4.3 TOA Outgoing Shortwave Radiation (rsut)

Figs. 5a and 5b provide regional plots of mean SW TOA flux and interannual variability for the month of March based upon all March months between 2000 and 2010. The regional 1°x1° standard deviation ranges from near zero at the poles to 40 W m^{-2} in the western tropical Pacific Ocean region. Considering all 1°x1° regions, the overall global regional standard deviation in SW TOA flux is 22 W m^{-2}, and the overall global mean SW TOA flux is 99.7 W m^{-2}.

The uncertainty in 1°x1° regional SW TOA flux is evaluated separately for 03/2000-06/2002 (Terra-Only period) and for 07/2002-12/2010 (Terra-Aqua period). To determine uncertainties for the Terra-Only period, we use data from the Terra-Aqua period and compare regional fluxes derived by applying diurnal corrections to fluxes from Terra SSF1deg with regional fluxes derived by averaging fluxes from Terra and Aqua determined using the SYN1deg interpolation method. SYN1deg combines CERES observations on Terra or Aqua with five geostationary instruments covering all longitudes between 60°S and 60°N, thus providing the most temporally and spatially complete CERES dataset for Terra or Aqua. Figs. 6a and 6b show maps of the regional bias and RMS error. The overall regional RMS error is 4 W m^{-2}. In stratocumulus regions, RMS differences are typically around 5 W m^{-2}, or approximately 5% of the regional mean value.

Uncertainties for the Terra-Aqua period are determined by comparing regional fluxes derived by applying diurnal corrections to the average of Terra and Aqua SSF1deg fluxes with average Terra and Aqua regional fluxes from SYN1deg. Results, in Figs. 7a and 7b, show much improvement over the Terra-only case in Fig. 6, with regional errors decreasing to 2.7 W m^{-2} overall and with errors less than 3 W m^{-2} in stratocumulus regions.

To place the above results into context, regional mean and RMS differences between Terra and Aqua SYN1deg SW TOA fluxes are provided in Figs. 8a and 8b. Overall, the RMS difference is 4.4 W m^{-2}. RMS differences greater than 10 W m^{-2} are evident over Africa, Tibet and over isolated regions in the Americas. Since the same geostationary data are used for both Terra and Aqua SYN1deg, why should there be any discrepancy? The regional discrepancies are mainly associated with the regional normalization of 3-hourly geostationary data to either Terra or Aqua CERES measurements. The time mismatch of up to 1.5 hours could cause differences in cloud conditions between the two measurements (Doelling et al. 2013). Consequently, a longitudinal striping pattern appears that is correlated with the time separation between the geostationary and sun-synchronous observations.

If we assume the overall uncertainty is due to: 1) the EBAF diurnal correction, 2) the combined sum of the Terra and Aqua SYN1deg SW regional fluxes, which is given by the RMS difference between Terra and Aqua SYN1deg divided by the square root of 2, and 3) CERES instrument calibration uncertainty of 1 W m^{-2} (1σ), the regional uncertainty of all-sky SW TOA flux for EBAF Ed2.7 for March 2000–June 2002 is estimated as $\text{sqrt}(4^2+4.4^2/2+1^2)$ or approximately 5 W m^{-2}, and for July 2002-December 2010 is estimated as $\text{sqrt}(2.7^2+4.4^2/2+1^2)$ or 4 W m^{-2}.

While the diurnal corrections applied to SSF1deg fluxes do introduce a slight increase in regional SW TOA flux uncertainty, they dramatically improve the EBAF record by minimizing the impact of geostationary satellite artifacts, especially with respect to temporal regional trends. As an example, Figs. 9a and 9b show regional trends in SW TOA flux from EBAF Ed2.6 and SYN1deg for March 2000–December 2010. In Fig. 9b, vertical lines corresponding to geostationary satellite boundaries are clearly visible around 30°E, 100°E, 180°E, 105°W and 40°W. The geostationary artifacts are more pronounced over Africa and Asia but also show up to the east of South America. In contrast, the geostationary artifacts are largely absent in Fig. 5a, which is based upon EBAF Ed2.6 data. Figs. 10a and 10b provide SW TOA flux anomaly differences between SYN1deg and SSF1deg as well as EBAF and SSF1deg for 60°S-60°N (Fig. 10a) and for the same latitude range but with longitude restricted to 101.5°E–140°E (Fig. 10b). The latter region covers much of the Western Tropical Pacific Ocean region, Indonesia, and East Asia. In both cases, the SYN1deg results show a sharp decline relative to SSF1deg reaching 0.4 W m^{-2} per decade for 60°S-60°N and 1.8 W m^{-2} per decade in the smaller region. In contrast, the EBAF Ed2.6 results remain well within 0.1 W m^{-2} per decade of SSF1deg for both cases, while still accounting for the diurnal cycle.

Table 1 compares global TOA averages for EBAF Ed2.7 with earlier versions of the product. All-sky SW TOA flux in Ed2.7 is 0.3 W m^{-2} greater than Ed1.0 and 0.1–0.2 W m^{-2} greater than Ed2.5. The main difference between all-sky SW TOA fluxes in EBAF Ed2.7 and Ed2.5 is that Ed2.7 uses the methodology described in Section 3, while EBAF Ed2.5 is derived from SYN1deg-lite Ed2.5 (a preliminary release of SYN1deg Ed3), which relies explicitly on geostationary satellite measurements to complete the diurnal cycle. Another difference that applies to all TOA flux variables is that EBAF Ed2.7 applies geodetic weighting when averaging globally, while geocentric weighting is assumed in EBAF Ed2.5 and EBAF Ed1.0.

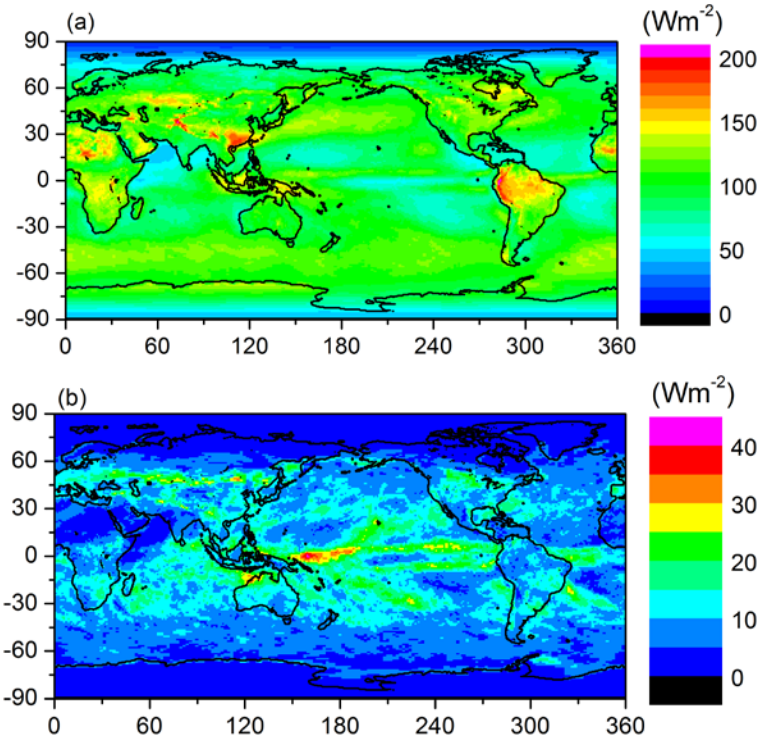

Figure 5. (a) Average and (b) standard deviation of SW TOA flux determined from all March months from 2000–2010 using the CERES EBAF Ed2.6 product.

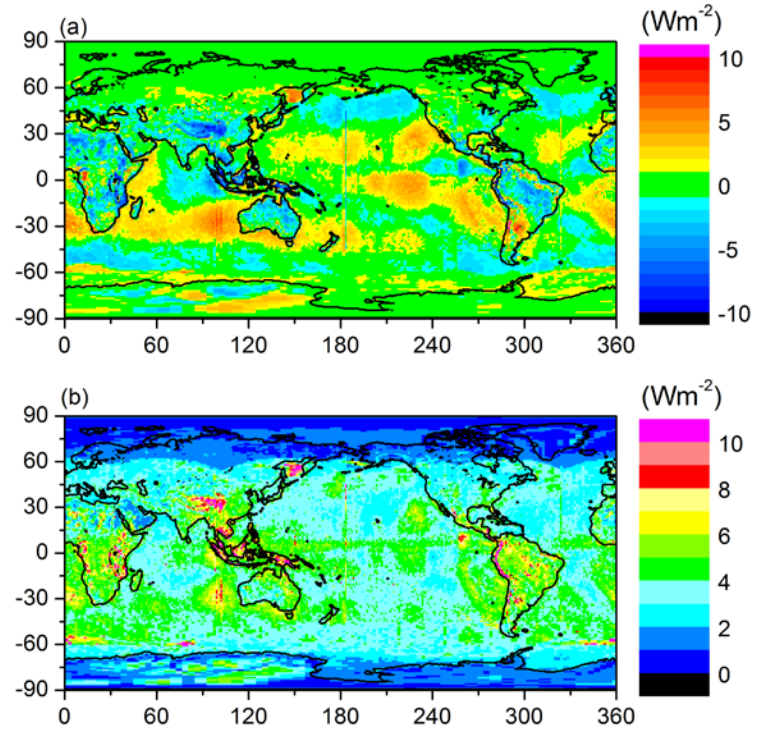

Figure 6. (a) Bias and (b) RMS difference between SW TOA fluxes derived by applying diurnal corrections to Terra SSF1deg-lite Ed2.6 and TOA fluxes from the average of Terra and Aqua SYN1deg-lite.

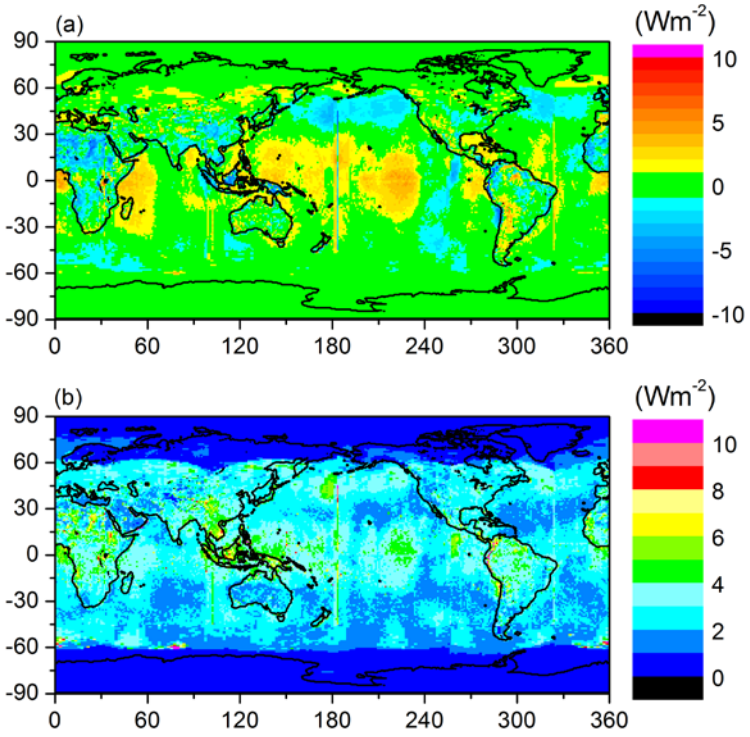

Figure 7. Same as Fig. 6 but after applying diurnal corrections to combined Terra+Aqua SSF1deg-lite Ed2.6 fluxes.

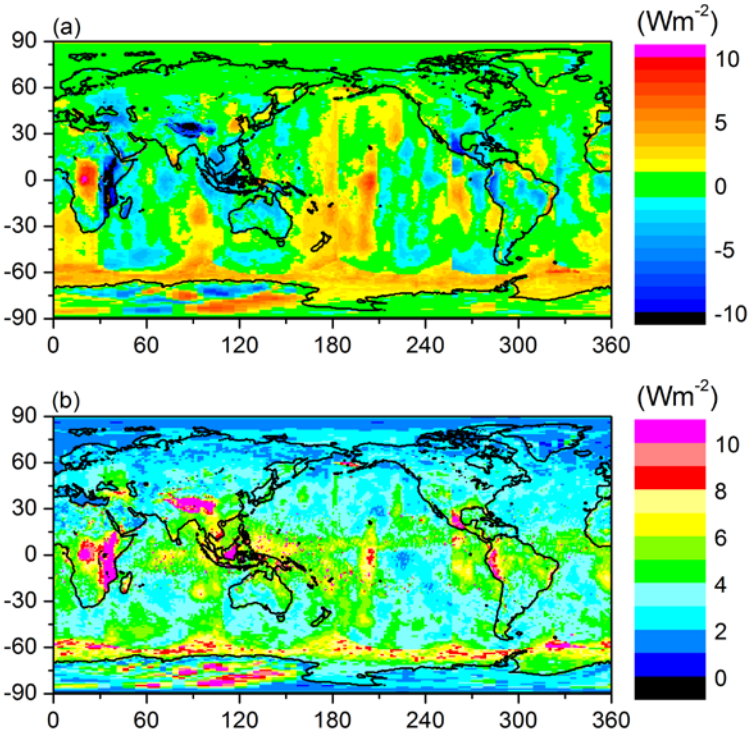

Figure 8. (a) Mean and (b) RMS difference between SW TOA fluxes from CERES Terra and CERES Aqua SYN1deg-lite Ed2.6 data products.

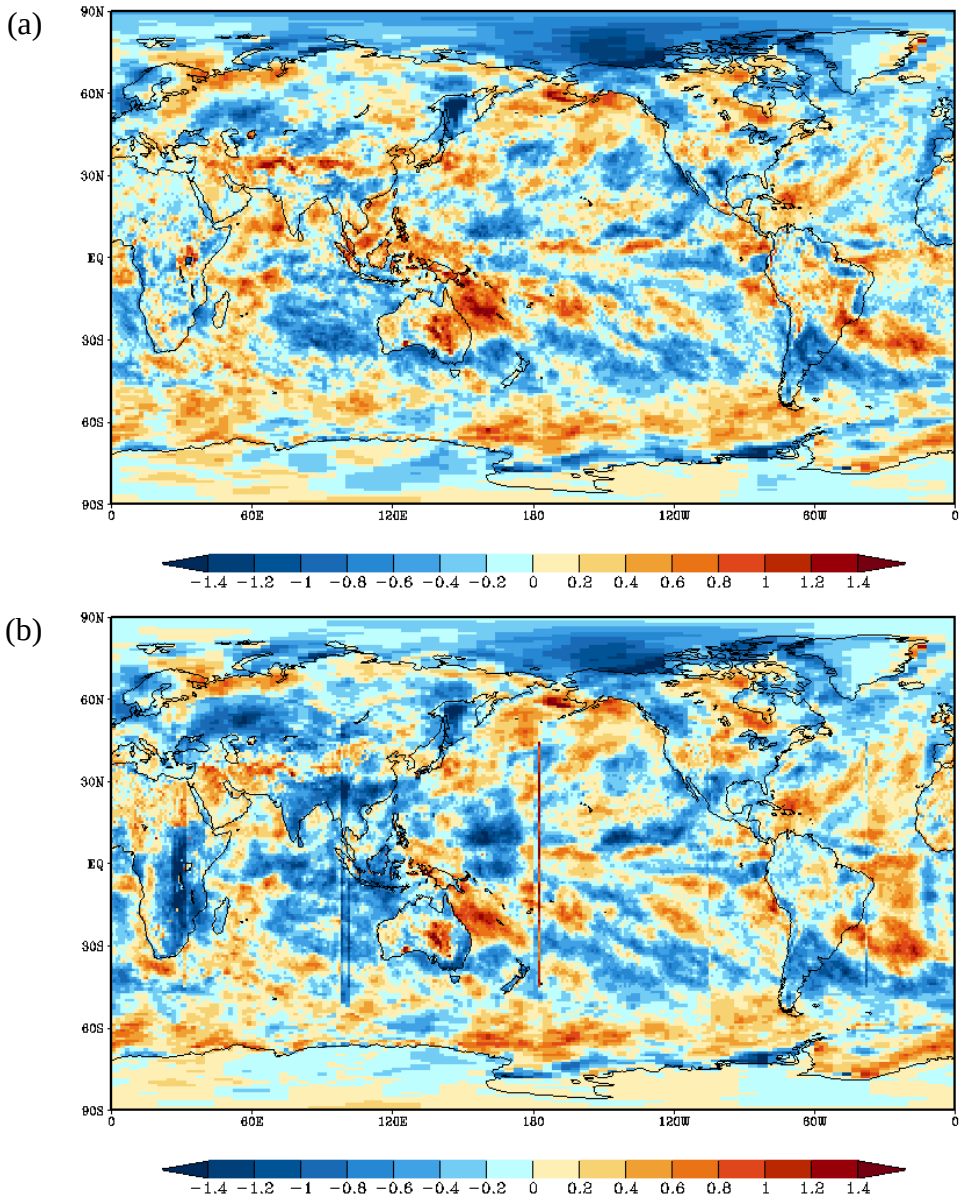

Figure 9. Regional trends (W m^{-2} per decade) in SW TOA flux for March 2000-December 2010 from (a) EBAF Ed2.6 and (b) SYN1deg-lite Ed2.6.

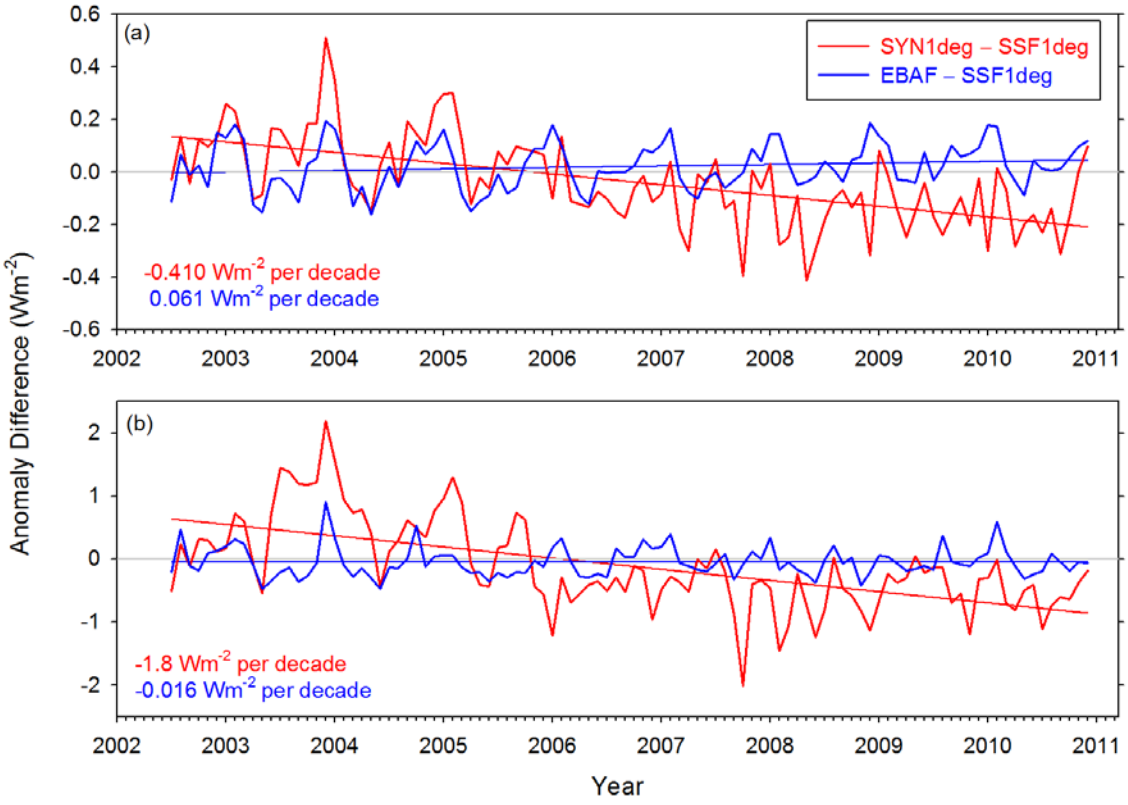

Figure 10. SW TOA flux anomaly difference between SYN1deg-lite Ed2.6 and SSF1deg-lite Ed2.6 and between EBAF and SSF1deg-lite Ed2.6 for (a) 60°S-60°N, and (b) the western sector of the region covered by GMS-5, GOES-9, and MTSAT-1R geostationary satellites (60°S–60°N, 101.5°E–140°E) for July 2002–December 2010. Straight lines correspond to least-square fits through the anomaly difference curves. Slopes are in units of W m^{-2} per decade.

4.4 TOA Outgoing Clear-Sky Shortwave Radiation (rsutcs)

Figs. 11a and 11b provide regional plots of mean clear-sky SW TOA flux and interannual variability for the month of March based upon all March months between 2000 and 2010. The regional 1°x1° standard deviation ranges from near zero over remote ocean regions to 35 W m^{-2} over mid-latitude land regions, associated with seasonal snow. Considering all 1°x1° regions, the overall global regional standard deviation in clear-sky SW TOA flux is 22 W m^{-2}, and the overall global mean is 54 W m^{-2}.

The uncertainty in 1°x1° regional clear-sky SW TOA flux is determined from calibration uncertainty and errors in narrow-to-broadband conversion, radiance-to-flux conversion, time-space averaging, and scene identification. For CERES, calibration uncertainty is 1% (1σ), which for a typical global mean clear-sky SW flux corresponds to ≈0.5 W m^{-2}. Figs. 12a and 12b show the regional distribution of the correction used to offset the regional narrow-to-broadband error. This is derived by applying narrow-to-broadband regressions to MODIS visible radiances for completely cloud-free CERES footprints and then comparing the estimated broadband flux with CERES. The overall bias is 0.2 W m^{-2}, and the regional RMS difference is 0.65 W m^{-2}. Assuming a 50% error in the correction, the narrowband-to-broadband contribution to regional

uncertainty becomes 0.3 W m^{-2}. For clear-sky SW TOA flux, the radiance-to-flux conversion error contributes 1 W m^{-2} to regional RMS error (Loeb et al. 2007), and time-space averaging adds 2 W m^{-2} uncertainty. The latter is based upon an estimate of the error from TRMM-derived diurnal albedo models that provide albedo dependence upon scene type (Loeb et al. 2003). In EBAF, "clear-sky" is defined as cloud-free at the MODIS pixel scale (1 km). A pixel is identified as clear using spectral MODIS channel information and a cloud mask algorithm (Minnis et al. 2011). Based upon a comparison of SW TOA fluxes for CERES footprints identified as clear according to MODIS but cloudy according to CALIPSO with TOA fluxes from footprints identified as clear according to both MODIS and CALIPSO, Sun et al. (2011) found that footprints with undetected subvisible clouds reflect 2.5 W m^{-2} more SW radiation compared to completely cloud-free footprints and occur in approximately 50% of footprints identified as clear by MODIS. This implies an error of 1.25 W m^{-2} due to misclassification of clear scenes. The total error in TOA outgoing clear-sky SW radiation in a region is estimated as sqrt(0.5^2+0.3^2+1^2+2^2+1.25^2) or approximately 2.6 W m^{-2}.

Table 1 compares global TOA averages for EBAF Ed2.7 with earlier versions of the product. Clear-sky SW TOA flux in Ed2.7 is 0.3 W m^{-2} lower than Ed1.0 and within 0.2 W m^{-2} of Ed2.5 and Ed2.6. The main difference between EBAF Ed2.7 and Ed2.5 is that Ed2.7 applies geodetic weighting when averaging globally while geocentric weighting is assumed in EBAF Ed2.5. In EBAF Ed1.0, geocentric weighting is assumed and the methodology for time-space averaging differs from versions Ed2.5 and higher. Time-space averaging for the latter is now based upon the same code that is used for clear-sky SW TOA fluxes in the SSF1deg product.

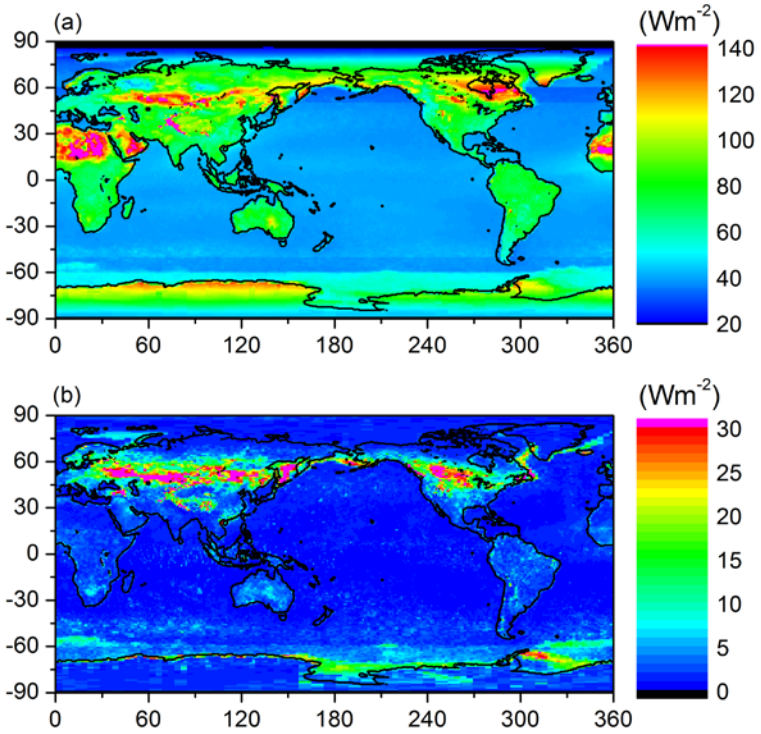

Figure 11. (a) Average and (b) standard deviation of clear-sky SW TOA flux determined from all March months from 2000–2010 using the CERES EBAF Ed2.6 product.

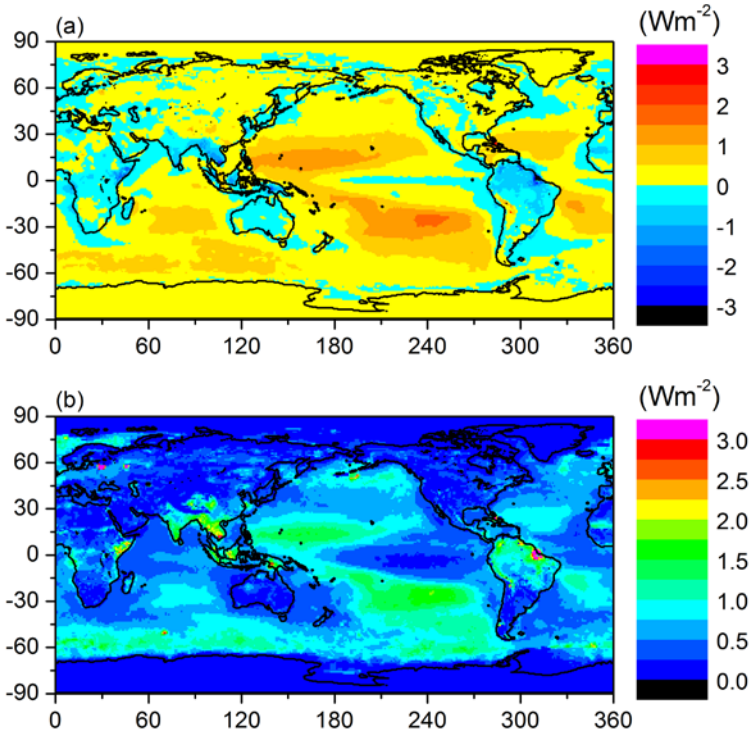

Figure 12. (a) Bias and (b) RMS difference between high-resolution clear-sky SW TOA fluxes derived with and without corrections for regional narrow-to-broadband error.

5. Considerations for Model-Observation Comparisons

Since TOA flux represents a flow of radiant energy per unit area and varies with distance from the earth according to the inverse-square law, a reference level is also needed to define satellite-based TOA fluxes. From theoretical radiative transfer calculations using a model that accounts for spherical geometry, the optimal reference level for defining TOA fluxes in radiation budget studies for the earth is estimated to be approximately 20 km. At this reference level, there is no need to explicitly account for horizontal transmission of solar radiation through the atmosphere in the earth radiation budget calculation. In this context, therefore, the 20-km reference level corresponds to the effective radiative "top of atmosphere" for the planet. Since climate models generally use a plane-parallel model approximation to estimate TOA fluxes and the earth radiation budget, they implicitly assume zero horizontal transmission of solar radiation in the radiation budget equation and do not need to specify a flux reference level. By defining satellite-based TOA flux estimates at a 20-km flux reference level, comparisons with plane-parallel climate model calculations are simplified since there is no need to explicitly correct plane-parallel climate model fluxes for horizontal transmission of solar radiation through a finite atmosphere. For a more detailed discussion of reference level, please see Loeb et al. (2002).

5.1 TOA Outgoing Longwave Radiation (rlut)

As noted in Section 3, the CERES monthly LW TOA fluxes account for diurnal cycle. Since the CERES instruments provide global coverage daily, monthly mean regional fluxes are based upon complete daily samples over the entire globe.

5.2 TOA Outgoing Clear-Sky Longwave Radiation

Clear-sky TOA fluxes in EBAF Ed2.7 are provided for clear regions within CERES footprints from MODIS pixels identified as clear at 1-km spatial resolution. This definition differs from what is used in the standard CERES data products (SSF1deg and SYN1deg), which only provide clear-sky fluxes in regions that are completely cloud-free at the CERES footprint scale. LW TOA fluxes for clear-sky regions identified at the higher spatial resolution are on average 2.4 W m^{-2} lower overall compared to the coarser resolution footprint case, and the regional RMS difference is 4 W m^{-2}. Users should be aware that both of these definitions of "clear-sky" might differ from what is used in climate model output. Many models compute clear-sky radiative fluxes in each column, regardless of whether the column is clear or cloudy. Sohn et al. (2006) note that differences in how clear-sky is defined in model output and observations can lead to regional LW TOA flux differences of up to 12 W m^{-2}. Because cloudy columns are typically more moist and cooler than columns that are cloud-free, model-based clear-sky SW TOA fluxes may be biased low compared to the EBAF clear-sky LW observations.

Clear-sky monthly mean LW TOA fluxes are determined by inferring TOA fluxes at each hour of the month and averaging. Clear-sky LW TOA fluxes between observation times are determined by linear interpolation of LW fluxes over ocean and by applying a half-sine fit during daytime and nighttime over land and desert. Therefore, we do not explicitly account for changes in the physical properties of the scene during all hours of the day. Since the CERES instruments provide global coverage daily, monthly mean regional fluxes are based upon complete daily samples over the entire globe.

5.3 TOA Outgoing Shortwave Radiation (rsut)

As noted in the Section 3, the CERES monthly SW TOA fluxes account for diurnal cycle. Since the CERES instruments provide global coverage daily, monthly mean regional fluxes are based upon complete daily samples over the entire globe.

Users interested in utilizing CERES EBAF Ed2.7 to explore short-term trends in SW TOA flux are cautioned that CERES Terra observations are used for the period from March 2000-June 2002, while both CERES Terra and Aqua are used from July 2002 onwards. Consequently, there can be a small artificial discontinuity in the data in July 2002 due to the introduction of Aqua.

When the solar zenith angle is greater than 90°, twilight flux (Kato and Loeb 2003) is added to the outgoing SW flux in order to take into account the atmospheric refraction of light. The magnitude of this correction varies with latitude and season and is determined independently for all-sky and clear-sky conditions. In general, the regional correction is less than 0.5 W m^{-2}, and the global mean correction is 0.2 W m^{-2}. Due to the contribution of twilight, there are regions near the terminator in which outgoing SW TOA flux can exceed the incoming solar radiation. Users should be aware that in these cases, albedos (derived from the ratio of outgoing SW to incoming solar radiation) exceed unity.

5.4 TOA Outgoing Clear-Sky Shortwave Radiation (rsutcs)

Clear-sky TOA fluxes in EBAF Ed2.7 are provided for clear regions within CERES footprints from MODIS pixels identified as clear at 1-km spatial resolution. This definition differs from what is used in the standard CERES data products (SSF1deg and SYN1deg), which only provide clear-sky fluxes in regions that are completely cloud-free at the CERES footprint scale. SW TOA fluxes for clear-sky regions identified at the higher spatial resolution are on average 1.6 W m^{-2}

higher overall compared to the coarser resolution footprint case, and the monthly mean regional RMS difference is 6 W m^{-2}. Users should be aware that both of these definitions for "clear-sky" might differ from what is used in climate model output. Many models compute clear-sky radiative fluxes in each column, regardless of whether the column is clear or cloudy. As a result, model-based clear-sky SW TOA fluxes may be biased high compared to the EBAF clear-sky SW observations.

Clear-sky monthly mean SW TOA fluxes are determined by inferring TOA fluxes at each hour of the month and averaging. Clear-sky SW TOA fluxes between observation times are determined from the observed fluxes by using scene-dependent diurnal albedo models to estimate how TOA albedo (and therefore flux) changes with solar zenith angle for each local time, assuming the scene properties remain invariant throughout the day. Therefore, we do not explicitly account for changes in the physical properties of the scene (e.g., aerosols, surface properties) during the course of the day. Since the CERES instruments provide global coverage daily, monthly mean regional fluxes are based upon complete daily samples over the entire globe.

When the solar zenith angle is greater than 90°, twilight flux (Kato and Loeb 2003) is added to the outgoing SW flux in order to take into account the atmospheric refraction of light. The magnitude of this correction varies with latitude and season and is determined independently for all-sky and clear-sky conditions. In general, the regional correction is less than 0.5 W m^{-2}, and the global mean correction is 0.2 W m^{-2}. Due to the contribution of twilight, there are regions near the terminator in which outgoing SW TOA flux can exceed the incoming solar radiation. Users should be aware that in these cases, albedos (derived from the ratio of outgoing SW to incoming solar radiation) exceed unity.

6. Instrument Overview

See the first paragraph of Section 3 for an overview of the CERES instruments on the Terra and Aqua satellites.

7. References

The full version of CERES EBAF Ed2.7 is available from the following ordering site:

http://ceres.larc.nasa.gov/order_data.php

Doelling, D. R., N. G. Loeb, D. F. Keyes, M. L. Nordeen, D. Morstad, C. Nguyen, B. A. Wielicki, D. F. Young, and M. Sun, 2013: Geostationary enhanced temporal interpolation for CERES flux products. *J. Atmos. Oceanic Technol*., **30**, 1072-1090.

Hansen, J. et al., 2005: Earth's energy imbalance: confirmation and implications. *Science*, **308**, 1431–1435.

Kato, S., and N. G. Loeb, 2003: Twilight irradiance reflected by the earth estimated from Clouds and the Earth's Radiant Energy System (CERES) measurements. *J. Climate*, **16**, 2646–2650.

Kato, S., and N. G. Loeb, 2005: Top-of-atmosphere shortwave broadband observed radiance and estimated irradiance over polar regions from Clouds and the Earth's Radiant Energy System (CERES) instruments on Terra. *J. Geophys. Res.*, **110**, doi:10.1029/2004JD005308.

Loeb, N. G., K. J. Priestley, D. P. Kratz, E. B. Geier, R. N. Green, B. A. Wielicki, P. O. R. Hinton, and S. K. Nolan, 2001: Determination of unfiltered radiances from the Clouds and the Earth's Radiant Energy System (CERES) instrument. *J. Appl. Meteor*., **40**, 822–835.

Loeb, N. G., S. Kato, and B. A. Wielicki, 2002: Defining top-of-atmosphere flux reference level for Earth Radiation Budget studies. *J. Climate*, **15**, 3301-3309.

Loeb, N. G., N. M. Smith, S. Kato, W. F. Miller, S. K. Gupta, P. Minnis, and B. A. Wielicki, 2003: Angular distribution models for top-of-atmosphere radiative flux estimation from the Clouds and the Earth's Radiant Energy System instrument on the Tropical Rainfall Measuring Mission Satellite. Part I: Methodology. *J. Appl. Meteor*., **42**, 240–265.

Loeb, N. G., S. Kato, K. Loukachine, and N. M. Smith, 2005: Angular distribution models for top-of-atmosphere radiative flux estimation from the Clouds and the Earth's Radiant Energy System instrument on the Terra satellite. Part I: Methodology. *J. Atmos. Oceanic Technol*., **22**, 338–351.

Loeb, N. G., W. Sun, W. F. Miller, K. Loukachine, and R. Davies, 2006: Fusion of CERES, MISR and MODIS measurements for top-of-atmosphere radiative flux validation. *J. Geophys. Res.*, **111**, D18209, doi:10.1029/2006JD007146.

Loeb, N. G., S. Kato, K. Loukachine, and N. Manalo-Smith, 2007: Angular distribution models for top-of-atmosphere radiative flux estimation from the Clouds and the Earth's Radiant Energy System instrument on the Terra satellite. Part II: Validation. *J. Atmos. Oceanic Technol.*, **24**, 564-584.

Loeb, N. G., B. A. Wielicki, D. R. Doelling, G. L. Smith, D. F. Keyes, S. Kato, N. M. Smith, and T. Wong, 2009: Towards optimal closure of the earth's top-of-atmosphere radiation budget. *J. Climate*, **22**, 748-766.

Loeb, N. G., J. M. Lyman, G. C. Johnson, R. P. Allan, D. R. Doelling, T. Wong, B. J. Soden, and G. L. Stephens, 2012a: Observed changes in top-of-the-atmosphere radiation and upper-ocean heating consistent within uncertainty. *Nat. Geosci*., **5**, doi:10.1038/ngeo1375.

Loeb, N. G., S. Kato, W. Su, T. Wong, F. G. Rose, D. R. Doelling, and J. Norris, 2012b: Advances in understanding top-of-atmosphere radiation variability from satellite observations. *Surv. Geophys*., **33**, doi: 10.1007/s10712-012-9175-1.

Lyman, J.M., and G.C. Johnson, 2008: Estimating annual global upper-ocean heat content anomalies despite irregular in situ ocean sampling. *J. Climate*, **21**, 5629–5641.

Minnis P., S. Sun-Mack, D. F. Young, P. W. Heck, D. P. Garber, Y. Chen, D. A. Spangenberg, R. F. Arduini, Q. Z. Trepte, W. L. Smith, Jr., J. K. Ayers, S. C. Gibson, W. F. Miller, G. Hong, V. Chakrapani, Y. Takano, K.-N. Liou, Y. Xie, and P. Yang, 2011: CERES Edition-2 cloud property retrievals using TRMM VIRS and Terra and Aqua MODIS data--Part I: Algorithms. *IEEE Trans. Geosci. Remote Sens*., **49**, 4374-4400.

Purkey, S. G., and G. C. Johnson, 2010: Warming of global abyssal and deep southern ocean waters between the 1990s and 2000s: contributions to global heat and sea level rise budgets. *J. Climate*, **23**, 6336–6351.

Roemmich, D. et al., 2009: Argo: the challenge of continuing 10 years of progress. *Oceanography*, **22**, 46–55.

Sohn, B.-J., J. Schmetz, R. Stuhlmann, and J.-Y. Lee, 2006: Dry bias in satellite-derived clear-sky water vapor and its contribution to longwave cloud radiative forcing. *J. Climate*, **19**, 5570-5580.

Sun, W., G. Videen, S. Kato, B. Lin, C. Lukashin, and Y. Hu, 2011: A study of subvisual clouds and their radiation effect with a synergy of CERES, MODIS, CALIPSO, and AIRS data, *J. Geophys. Res.,* **116**, D22207, doi:10.1029/2011JD016422.

Thomas S., K. J. Priestley, N. Manalo-Smith, N. G. Loeb, P. C. Hess, M. Shankar, D. R. Walikainen, Z. P. Szewcyzk, R. S. Wilson, D. L. Cooper, 2010: Characterization of the Clouds and the Earth's Radiant Energy System (CERES) sensors on the Terra and Aqua spacecraft. *Proc. SPIE*, Earth Observing Systems XV, Vol. 7807, 780702, August 2010.

Trenberth, K. E., 2009: An imperative for climate change planning: tracking Earth's global energy. *Current Opinion in Environmental Sustainability*, **1**, 19–27.

8. Dataset and Document Revision History

Rev 0 – 09 Aug 2011 – This is a new document/dataset

Rev 1 – 05 Mar 2012 – Updated to Edition2.6r. EBAF Ed2.6r corrects a code error in the calculation of global mean quantities in EBAF Ed2.6. Also updates temporal extent to 06/2011 from 12/2010. This version also updates some of the references.

Rev 2 – 06 Jun 2012 – Updated temporal extent to 12/2011 from 06/2011.

Rev 3 – 01 Nov 2012 – Updated temporal extent to 06/2012 from 12/2011.

Rev 4 – 28 Aug 2013 – Updated to Edition2.7 to improve clear-sky SW and LW TOA fluxes over snow and sea-ice. Corrects small error in all-sky regions falling in adjacent time zones. Updated the temporal extent to 02/2013 from 06/2012.

Rev 5 – 18 Sep 2013 – Updated temporal extent to 04/2013 from 02/2013.